Hyperdimensional Computing with Multi-Scale Local Binary Patterns for Scalp EEG-based Epileptic Seizure Detection

Yipeng Du, Yuan Ren, Ngai Wong, *Senior Member, IEEE,* and Edith C. H. Ngai, *Senior Member, IEEE*

***Abstract*—Epilepsy is a common condition that causes frequent seizures, significantly impacting patients' daily lives. Non-invasive EEG is an effective tool for detecting seizure onset. Wearable EEG devices enable real-time monitoring and timely intervention but pose new algorithmic challenges on small model weight sizes and limited training data. Brain-inspired hyperdimensional computing (HDC) presents a potential solution for its small weight size and quick learning ability. Combining local binary pattern (LBP) codes with HDC can capture dynamic features in EEG time series. However, traditional LBP features may not offer sufficient robustness for trend modeling due to their high localization on individual samples, particularly on low-amplitude and non-stationary scalp EEG signals. To address the above challenges, this paper proposes a multi-scale LBP-based HDC (MSLBP-HDC) approach for scalp EEG analysis. Unlike traditional LBP-based HDC focusing only on the local change trend, the designed MSLBP-HDC extracts dynamic features at different time resolutions to detect abnormal cortical oscillations. The lengths of multiple temporal scales in MSLBP-HDC are determined based on the duration of spikes. Our results demonstrate that MSLBP-HDC has the highest specificity for all test seizure types and achieves competitive macroaveraging accuracy with the smallest model weight size in detection, compared to advanced deep learning, support vector machine, and HDC methods. Regarding few-shot learning performance, MSLBP-HDC outperforms existing approaches and achieves high accuracy using only 1% of the training data. Moreover, feature interpretability analysis from space and time domains highlights that MSLBP-HDC successfully extracts seizure-relevant features rather than noise or artifacts, ensuring the algorithm's reliability.**

***Index Terms*—Hyperdimensional computing, scalp EEG, seizure detection, wearable devices, local binary pattern, feature interpretability analysis.**

I. Introduction

Epilepsy is a chronic brain disorder caused by abnormal firing of neurons [1], which occurs when the balance between excitation and inhibition of patients' neurons is disrupted [2]. As one of the most common neurological diseases, approximately 1% of the world's population is diagnosed with epilepsy [3]. Rapid and accurate detection of seizures is critical for treatment, dose control, and prognosis assessment [4]. Non-invasive Electroencephalogram (EEG) can reveal obvious abnormal activities in patients with seizures through electrodes attached to the scalp surface [5]. Given the inherent uncertainty of epilepsy, the combination of wearable EEG devices and Internet-of-Things (IoT) technology can provide real-time monitoring and timely interventions [6], [7]. Thus, developing a scalp EEG-based automatic epilepsy detection system on portable devices will significantly reduce the risk of patient injury and improve the overall quality of life [8].

Epilepsy detection tasks on wearable EEG devices pose new challenges to the algorithm design. The non-stationary and low-amplitude characteristics of scalp EEG signals make them susceptible to noise and artifacts during real-time monitoring on portable devices, resulting in reduced detection accuracy. In actual scenarios, different patients have various types of seizures with different features, such as the duration of spikes [9]. The algorithms must be robust enough to handle feature extraction modes for different seizure types. The models should also have a small weight size to minimize computation overhead and improve detection speed in embedded systems. Few-shot learning is essential for the algorithms considering the difficulty of epileptic EEG acquisition. The models should be able to generalize and detect new seizures using only a small amount of annotated data. Additionally, the algorithms need high reliability to ensure that epilepsy-related features are extracted rather than noise or artifacts for accurate detection, which is critical for medical applications. Therefore, designing a reliable algorithm is crucial for scalp EEG-based seizure detection systems on wearable devices.

To meet the above requirements, recent studies have made significant progress in automatic epilepsy detection tasks by employing machine learning methods. Traditional machine learning methods rely on prior knowledge for feature extraction and feature selection to realize the recognition of different brain states, i.e., ictal and interictal states. Commonly used models include support vector machine (SVM) [10], [11], k-nearest neighbor (KNN) classifier [12], and random forest (RF) classifier [13]. The performance of traditional machine learning methods largely depends on the quality of features extracted using domain knowledge. However, this feature extraction mode has limitations in terms of the generalization ability of the algorithms, making models difficult to apply to complex and dynamic real-world environments.

Deep learning methods jointly learn feature representation and classification from data with the help of deep structure, thus avoiding the limitations of manual feature extraction and

This work was supported in part by the Theme-based Research Scheme (TRS) project T45-701/22-R of the Research Grants Council (RGC), Hong Kong Special Administrative Region (HKSAR). *(Corresponding author: Edith C. H. Ngai.)*

Yipeng Du, Yuan Ren, Ngai Wong and Edith C. H. Ngai are with the Department of Electrical and Electronic Engineering, Faculty of Engineering, The University of Hong Kong, Hong Kong, China (e-mail: yipengdu@connect.hku.hk; renyuan@eee.hku.hk; nwong@eee.hku.hk; chngai@eee.hku.hk).

improving epilepsy detection performance. In the realm of epileptic EEG analysis, supervised learning methods such as convolutional neural networks (CNNs) [14], [15], [16], long short-term memory networks (LSTMs) [17], [18], [19], and hybrid models [20], [21], [22] have demonstrated promising results when trained on annotated data [23]. Conversely, unsupervised learning methods, particularly autoencoders [24], [25], [26], excel at capturing latent features associated with epilepsy occurrences in EEG signals. By learning low-dimensional representations of the data, autoencoders enable automated seizure detection even in the absence of labeled training data. Although deep learning models can get high accuracy on the test datasets, in practical applications, deep neural networks have many limitations on portable devices as they cannot meet all the above algorithm requirements. Firstly, data-driven neural networks have to accumulate a large amount of patients' seizure data to realize high-precision seizure detection, which is difficult to achieve in the real world due to the uncertainty of seizures. Secondly, the large model weight size of deep learning models imposes a heavy burden on the hardware, making it hard to conduct real-time seizure detection on wearable devices. Finally, due to the black-box nature of deep neural networks, the reliability of the algorithms cannot be guaranteed, which limits their large-scale application in the medical field.

Hyperdimensional computing (HDC), as a brain-inspired vector-symbolic computational model, can meet the above algorithm requirements for epileptic EEG analysis on portable devices [27]. Inspired by the cognitive models [28], HDC applies hypervectors with high dimensionality and randomness to represent the cortical oscillations recorded on EEG. The data representations of different brain states are realized through three operations on hypervectors: bundling, binding, and permutation. In the item memory of HDC, the hypervectors are randomly generated and exhibit quasi-orthogonality due to their high dimensionality. Three operations, namely bundling, binding, and permutation, are applied to these hypervectors to achieve the representation of various brain states. The bundling operation involves pointwise addition, which generates a hypervector similar to all the input hypervectors. Moreover, the binding operation, also known as pointwise multiplication, establishes relationships between the input hypervectors. In the binary HDC model, the XOR operation is utilized for binding operations. Another important operation is permutation, which generates a quasi-orthogonal hypervector by applying a permutation matrix to the input hypervector. Permutation allows for shuffling the input hypervector, and circular shifting is the most widely adopted method in permutation operations [29].

Different from the feature extraction mode of traditional machine learning methods, the high dimensionality of HDC introduces redundancy in the encoding process to reduce the impact of noise and artifacts. The generated holographic distributed representations enable the classification of ictal and interictal states by comparing similarities in hyperdimensional space. The HDC model, which has a small model weight size and high energy efficiency, is easy to implement and deploy on hardware to realize real-time epilepsy monitoring on wearable EEG devices [30]. Furthermore, the fast-learning property of HDC enables it to generalize and identify unlabeled EEG signals with limited annotated data, reducing the need for extensive training data.

Researchers have proposed various HDC methods for epilepsy detection based on scalp EEG and intracranial EEG (iEEG) signals. In terms of model structure, Pale *et al.* considered intra-class variability and developed a semi-supervised learning approach based on multi-centroid HDC model [31]. In [32], a hybrid model was constructed to leverage both personal and general HDC models, facilitating knowledge transfer between different datasets. Additionally, [33] and [34] introduced feature selection algorithms in HDC models for the analysis of iEEG and scalp EEG signals, respectively. Regarding input feature design, Asgarinejad *et al.* utilized raw signal amplitude as the input for HDC model [35]. In [36], various HDC encoding schemes were evaluated on both iEEG and scalp EEG signals, encompassing local binary pattern (LBP) feature [37], raw signal amplitude feature, frequency spectrum feature, and combinations of multiple features. Notably, by combining the principles of symbolic dynamics [38] with HDC, Burrello *et al.* achieved remarkable results in the iEEG-based seizure detection task [39]. In their proposed method, symbolic LBP codes were extracted from iEEG signals. And HDC was adopted to encode them into hyperdimensional space, enabling training and classification of hypervectors with different brain states. Experimental results demonstrated that the proposed scheme could quickly learn from a small number of seizures and perform seizure detection on iEEG signals. Furthermore, [40] showcased the superiority of LBP-based HDC model over other baseline models in terms of energy consumption and inference speed when performing epileptic iEEG analysis on embedded devices.

However, compared with the analysis of iEEG, the epilepsy monitoring of scalp EEG that this study focuses on poses a greater challenge to the algorithms. Scalp EEG is low in amplitude, so its analysis is more susceptible to noise and artifacts than iEEG. Moreover, due to the spatial averaging effect of the skull and dura [41], traditional LBP codes for iEEG are too localized on individual samples to be robust enough for detecting epilepsy in scalp EEG. Therefore, the current approach is inadequate in accurately monitoring various types of seizures in scalp EEG, especially when working with limited datasets.

To address the above problems, we propose a multi-scale LBP-based HDC (MSLBP-HDC) to improve the seizure detection performance of scalp EEG on wearable devices. Our contributions can be summarized as follows:

1) In MSLBP-HDC, the designed multi-scale LBP features can integrate multi-scale information from scalp EEG for seizure detection. By taking into account the duration of spikes, the lengths of various temporal scales in MSLBP-HDC are determined to extract dynamic features of different types of epilepsy. In addition, model ensemble is adopted to improve the accuracy and robustness of the HDC model on small datasets. Compared with traditional LBP-based HDC using a single limited temporal scale, MSLBP-HDC improves the accuracy by

3.03% under the same condition of using 9000 bits in hypervectors.

2) MSLBP-HDC, with its minimal model weight size, outperforms advanced deep learning methods and SVM on real clinical scalp EEG datasets, whether utilizing the entire training data or just 1% of it. And MSLBP-HDC shows superior and more stable performance than the existing HDC methods under different initialization seed settings in the item memory.
3) Feature interpretability analysis illustrates that MSLBP-HDC can successfully identify the location of focal epilepsy and the time of seizure onset, demonstrating the reliability of the algorithm. Furthermore, the analysis of embedded implementation highlights the exceptional energy efficiency of MSLBP-HDC, making it well-suited for wearable EEG devices.

II. Methods

In this section, we introduce the architecture of MSLBP-HDC, including the design of multi-scale LBP features to capture the dynamic changes of epileptic EEG and the application of HDC to classify ictal and interictal states of the brain in hyperdimensional space. Then we illustrate the feature interpretability methods for the hypervectors of MSLBP-HDC to identify the seizure onset in temporal and spatial dimensions, respectively.

Algorithm 1 Multi-Scale LBP Feature Extraction

Input:
Length of encoding window, D_W;
Number of scales in multi-scale LBP features, N_{scale};
Lengths of multi-scale LBP codes, $L_1^{msLBP}, ..., L_{N_{scale}}^{msLBP}$;
Lengths of average windows, $L_1^{AW}, ..., L_{N_{scale}}^{AW}$;
EEG samples of channel ch, $EEG_1^{ch}, ..., EEG_{D_W}^{ch}$.
Output:
Multi-scale LBP features, $msLBP$.

for $scale \leftarrow 1, 2, ..., N_{scale}$ **do**
  $L_S = (L_{scale}^{msLBP} + 1) * L_{scale}^{AW}$;
  for $t_1 \leftarrow L_S, L_S + 1, ..., D_W$ **do**
    for $t_2 \leftarrow 1, 2, ..., L_{scale}^{msLBP} + 1$ **do**
      $mean = 0$;
      $start = t_1 - L_S$;
      for $t_3 \leftarrow start + (t_2 - 1) \times L_{scale}^{AW} + 1, start + (t_2 - 1) \times L_{scale}^{AW} + 2, ..., start + t_2 \times L_{scale}^{AW}$ **do**
        $mean = mean + EEG_{t_3}^{ch}$;
      end for
      $S_{t_2}^{scale} = mean / L_{scale}^{AW}$;
    end for
    $\Delta = S_{2:L_{scale}^{msLBP}+1}^{scale} - S_{1:L_{scale}^{msLBP}}^{scale}$;
    $msLBP_{t_1}^{scale} = concat(\Delta > 0)$;
  end for
end for
return $msLBP$

A. The Architecture of MSLBP-HDC

To overcome the limitation of traditional LBP coding that only focuses on the local change trend of epileptic EEG, we propose the multi-scale LBP encoding to combine dynamic features of seizure over all electrodes at different temporal scales. Then HDC is adopted to generate the holographic distributed representation of brain states through multi-scale LBP features, which can effectively detect seizure from scalp EEG time series with a low signal-to-noise ratio. The processing pipeline of MSLBP-HDC is shown in Fig. 1, which includes three parts: feature extraction and HDC encoding, learning and classification of HDC, and post-processing.

1) Feature extraction and HDC encoding: When a patient has a seizure, the recorded real-time EEG will show obvious fluctuations in amplitude, such as spikes. Multi-scale LBP encoding, as a symbolic dynamics method, can transform epileptic EEG signals into bit strings while retaining useful information related to seizure, thus improving computational efficiency and reducing noise or artifacts' interference in feature extraction. LBP codes utilize binary bits to describe the trend of signal variations, making them a suitable input feature for binary HDC methods in feature analysis. In LBP codes, a binary value 1 is assigned when there is an upward trend between two consecutive time points of the signal, and 0 otherwise. For instance, if a signal exhibits an upward trend followed by a downward trend, the LBP code would output '10' as the signal feature input for analysis in the HDC model. The computation of multi-scale LBP features is illustrated in Algorithm 1.

The dynamic changes of epileptic EEG are captured using multi-scale LBP encoding. And this is achieved by controlling two parameters, namely L^{msLBP} and L^{AW}. L^{msLBP} is utilized to generate LBP codes of different lengths, which helps in analyzing epilepsy with varying durations. Since seizures can be variable between patients and even within a patient, LBP codes of different lengths can aid in useful feature extraction for different seizure types, enhancing the robustness of the detection algorithm. On the other hand, L^{AW} is applied to control signal resolutions during the LBP encoding process. Conventional LBP codes can only describe the variation trend between individual samples in EEG time series, but with L^{AW}, signal trends at different resolutions can be extracted into the LBP encoding, thus reducing the interference of noise and artifacts and improving the detection accuracy. Combining these two parameters generates different temporal scales of LBP codes that form the multi-scale LBP features.

Histogram of multi-scale LBP codes can reflect the emergence of patterns in the scalp EEG time series to classify ictal and interictal states of the brain. In our method, brain-inspired HDC theory is adopted to generate an approximate version of the multi-scale LBP histogram in hyperdimensional space, which can simplify computation using only binary components and save memory on wearable devices. Before encoding the multi-scale LBP histogram, the item memory is applied to allocate the quasi-orthogonal binary hypervectors to each EEG electrode and multi-scale LBP codes of each temporal scale. During the initialization of the item memory in HDC, we count the number of applied multi-scale LBP codes in advance

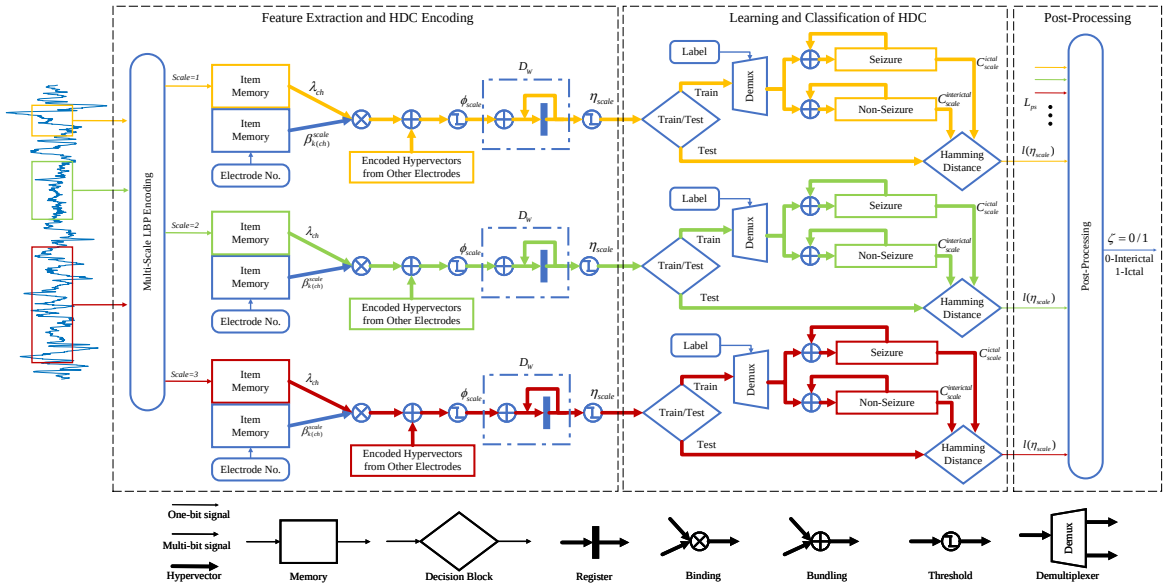

Fig. 1: Processing pipeline of multi-scale LBP-based HDC. It includes three parts: feature extraction and HDC encoding, learning and classification of HDC, and post-processing.

and construct unique binary hypervectors for each code. It is important to note that the hypervectors in the item memory are initialized randomly during the training stage and can be easily regenerated from the random seed by using cellular automaton [42]. The allocated hypervectors for EEG electrodes and multi-scale LBP codes can be defined as λ_{ch} and β_k^{scale}, where ch denotes the electrode and k represents the $k-th$ LBP code of multi-scale LBP codes at one temporal scale. The binary hypervectors λ_{ch} and β_k^{scale} satisfy the following conditions: $\lambda_1 \perp \lambda_2 ... \perp \lambda_{N_{ch}}$, and $\beta_1^{scale} \perp \beta_2^{scale} ... \perp \beta_{N_{LBP}}^{scale}$. The binding operation is employed to create associations between the hypervectors of the specific electrode and corresponding LBP code, i.e., $\lambda_{ch} \otimes \beta_{k(ch)}^{scale}$. For each temporal scale of multi-scale LBP codes, the spatial information of scalp EEG over all electrodes at time t can be encoded in hyperdimensional space via the bundling operation, and it can be written as,

$$\begin{aligned}\phi_{scale}[t] &= \sum_{ch=1}^{N_{ch}} \lambda_{ch} \otimes \beta_{k(ch)}^{scale}[t] \\ &= \lambda_1 \otimes \beta_{k(1)}^{scale}[t] + \lambda_2 \otimes \beta_{k(2)}^{scale}[t] + ... + \lambda_{N_{ch}} \otimes \beta_{k(N_{ch})}^{scale}[t].\end{aligned} \tag{1}$$

$\phi[t]$ is the holographic distributed representation of LBP information on all electrodes at time t. To encode the histogram of multi-scale LBP codes inside the window D_W, the bundling operation is applied to sum $\phi[t]$ hypervectors, $t \in [1, D_W]$. This process can be expressed as,

$$\begin{aligned}\eta_{scale} &= \left\langle \sum_{t=1}^{D_W} \phi_{scale}[t] \right\rangle \\ &= \langle \phi_{scale}[1] + \phi_{scale}[2] + ... + \phi_{scale}[D_W] \rangle ,\end{aligned} \tag{2}$$

where $\langle . \rangle$ indicates the sum of histogram hypervectors is thresholded and binarized based on the majority rule. For each temporal scale of multi-scale LBP codes, the corresponding η_{scale} can represent the seizure and non-seizure states of the brain from a specific feature space. After encoding, we can obtain the binary distributed hypervectors of multi-scale LBP codes, which can be written as $\{\eta_1, \eta_2, ..., \eta_{N_{scale}}\}$.

2) Learning and classification of HDC: In the training stage, an associative memory is constructed, and two hypervectors for each temporal scale, namely C_{scale}^{ictal} and $C_{scale}^{interictal}$, are stored to represent seizure and non-seizure states in hyperdimensional space. As shown in Fig. 1, the class hypervectors C_{scale} are updated based on the histogram hypervector η_{scale}. To generate multiple segments for training from the input EEG time series, we apply an encoding window with dimension D_W, and the encoding module of MSLBP-HDC encodes multi-scale LBP features for each segment as a set of binary hypervectors $\{\eta_1, \eta_2, ..., \eta_{N_{scale}}\}$. We then accumulate the η_{scale} with the same label into the corresponding class hypervectors C_{scale} using the bundling operation, i.e., $C_{scale} = C_{scale} + \eta_{scale}$. It should be noted that MSLBP-HDC only requires one training iteration to complete the construction of class hypervectors. After training, the updated C_{scale} are stored in the associative memory for subsequent classification.

During the inference stage, we obtain a set of hypervectors, denoted by $\{\eta_1, \eta_2, ..., \eta_{N_{scale}}\}$, for an unannotated segment from the encoding module of MSLBP-HDC. For each η_{scale}, we determine its label $l(\eta_{scale})$ by comparing its normalized Hamming distance to the class hypervectors, C_{scale}^{ictal} and $C_{scale}^{interictal}$, respectively. This process can be written as,

$$l(\eta_{scale}) = \begin{cases} 1, & \text{if} \quad hamdist(C_{scale}^{ictal}, \eta_{scale}) \leq \\ & \quad hamdist(C_{scale}^{interictal}, \eta_{scale}), \\ 0, & \text{otherwise}, \end{cases} \tag{3}$$

where $l(\eta_{scale}) = 1$ represents the ictal state and 0 means

interictal state. $hamdist(.)$ is the function to calculate the normalized Hamming distance and it can be expressed as,

$$hamdist(C,\eta) = \frac{1}{D}\sum_{d=1}^{D} 1_{C(d)\neq\eta(d)}, \tag{4}$$

where D is the dimension of binary hypervectors. Since each temporal scale in MSLBP-HDC generates a classification result $l(\eta_{scale})$ by comparing the distance with C_{scale} in the associate memory, the final detection result will be determined through the post-processing module by utilizing multiple results from different temporal scales.

3) Post-processing: To enhance the precision of epilepsy detection, MSLBP-HDC incorporates classification information from multiple segments across different temporal scales through model ensemble during the post-processing phase. The decision window with dimension L_{ps} is defined to jointly detect multiple scalp EEG segments, as depicted in Fig. 1. In the post-processing module, the majority rule is adopted, and the final decision result ζ is represented as follows,

$$\zeta = \begin{cases} ictal, & \text{if } \sum_{r=1}^{L_{ps}}\sum_{scale=1}^{N_{scale}} l(\eta_{scale}^{r}) >= \frac{L_{ps}\times N_{scale}}{2}, \\ interictal, & \text{otherwise,} \end{cases} \tag{5}$$

where η_{scale}^{r} is the hypervectors of the $r-th$ segment at one temporal scale in the decision window. L_{ps} is a trade-off between detection accuracy and latency. If L_{ps} is too large, MSLBP-HDC is able to achieve high performance with great latency. However, if L_{ps} is too small, the accuracy of MSLBP-HDC will be low, resulting in unreliable detection results.

B. Feature interpretability Analysis

Feature interpretability methods are the critical component of robust model validation procedures, which can inspect the behavior of machine learning models, ensuring their trustworthiness in sensitive domains such as autonomous driving and medical applications [43]. In this study, we adopt feature explainability techniques to explore the information contained in the features of MSLBP-HDC from both the time and space domains. Specifically, we analyze the relationship between encoded histogram hypervectors and focal seizure area concerning the spatial dimension. On the other hand, we investigate the correlation between binary distributed hypervectors of HDC and onset time regarding the temporal dimension. Additionally, we use t-distributed Stochastic Neighbor Embedding (t-SNE) to visualize the feature discriminability of different labels for specific seizure type, namely video-detected seizure without visual change in EEG [44].

1) Feature interpretability in spatial dimension: To analyze the feature explainability of MSLBP-HDC in the space domain, we bundle holographic distributed representations of multi-scale LBP codes at different times across each channel, generating corresponding histogram hypervectors denoted as $\alpha_{scale,ch}$. The encoding process of $\alpha_{scale,ch}$ can be written as,

$$\begin{aligned}\alpha_{scale,ch} &= \left\langle \sum_{t=1}^{D_S} \beta_{k(ch)}^{scale}[t] \right\rangle \\ &= \left\langle \beta_{k(ch)}^{scale}[1] + \beta_{k(ch)}^{scale}[2] + ... + \beta_{k(ch)}^{scale}[D_S] \right\rangle,\end{aligned} \tag{6}$$

where D_S refers to the length of the encoding window, and we set it to 20 s for this experiment. For the feature interpretability analysis, reliability is of utmost importance as it provides suggestions for diagnosis and subsequent treatment by medical professionals. In this case, we chose a signal length of 20 seconds for feature relevance calculation to ensure high reliability in identifying the seizure onset zone. EEG data from 180 s to 160 s before the seizure is encoded into a hypervector $\alpha_{scale,ch}^{interictal}$ to represent the interictal state of the brain. Similarly, we encode the time series within the initial 20 s of seizure onset into a hypervector $\alpha_{scale,ch}^{ictal}$ to represent the seizure state. The normalized Hamming distance between two hypervectors for each channel across all temporal scales in MSLBP-HDC, denoted as h_{ch}, is then calculated. It can be expressed by,

$$h_{ch} = \frac{1}{N_{scale}}\sum_{n=1}^{N_{scale}} hamdist(\alpha_{n,ch}^{ictal}, \alpha_{n,ch}^{interictal}). \tag{7}$$

h_{ch} integrates information from different temporal scales to improve the precision of feature interpretation. By comparing the Hamming distances h_{ch} of different EEG channels during ictal and interictal periods, this method can measure the degree of signal change at different locations in the brain during a seizure. Specifically, a larger h_{ch} indicates that the signal of this channel fluctuates greatly during the ictal period. Thus, this location is closer to the ictogenic brain regions. During an interictal state, there is no noticeable difference between the hypervectors extracted from the EEG signals, resulting in a smaller Hamming distance. However, during a seizure, the EEG signals exhibit noticeable fluctuations, which are captured by the hypervectors extracted from MSLBP-HDC. As a result, these hypervectors differ significantly from those in the interictal state, resulting in a larger Hamming distance. In addition, to show the degree of EEG signal change during the interictal state, we encode the EEG data from 160 s to 140 s before the seizure into a hypervector and calculate its normalized Hamming distance with $\alpha_{scale,ch}^{interictal}$ for each channel across all temporal scales.

2) Feature interpretability in temporal dimension: Similar to feature explainability in the space domain, the interpretability of features in the temporal dimension analyzes changes in hypervectors over time during epilepsy occurrences. We use 0.5 s as the length of D_W in MSLBP-HDC encoding module to extract hypervectors $\{\eta_1, \eta_2, ..., \eta_{N_{scale}}\}$ from scalp EEG segments, for both ictal and interictal periods. Temporal changes in MSLBP-HDC features during seizures are determined by calculating the normalized Hamming distance between $\eta_{scale}[t]$ at different times and the interictal hypervectors $\eta_{scale}^{interictal}$ from 180 s to 179.5 s before the seizure. This process can be written as,

$$q_{scale}[t] = hamdist(\eta_{scale}[t], \eta_{scale}^{interictal}). \quad (8)$$

When a seizure occurs, the normalized Hamming distance q_{scale} between η_{scale}^{ictal} and $\eta_{scale}^{interictal}$ increases in the temporal dimension. Additionally, we visualize and compare feature changes across different temporal scales in MSLBP-HDC.

Unlike the black-box nature of deep learning models, we can employ straightforward feature interpretability methods to analyze the spatial and temporal characteristics of features in MSLBP-HDC. This enables the automatic determination of seizure location and onset time using scalp EEG signals, making feature explainability analysis of MSLBP-HDC a valuable tool not only for testing model robustness but also for providing clinical decision support to doctors in real-world scenarios.

III. Experiment Setup

A. Dataset Description

The performance of our proposed MSLBP-HDC method and the existing methods were evaluated on the public epileptic EEG dataset [45]. This dataset contained long-term scalp EEG recordings from patients at the Epilepsy Monitoring Unit of the American University of Beirut Medical Center. The multi-channel epileptic EEG time series were acquired using 21 scalp electrodes following the 10-20 electrode system, and the sampling rate was 500 Hz. Three seizure types were recorded in the dataset: complex partial seizure, electrographic seizure, and video-detected seizure without visual changes over EEG. Due to contact noise in the Pz and Cz channels of a single patient, which prevented normal EEG signal acquisition, we excluded these channels for that patient. In addition, we uniformly excluded specific channels (Pz and Cz channels) from all participants in the experiment. We performed this operation based on the following three reasons. Firstly, by removing the same channels across all participants, we ensured data consistency, thereby promoting fairness in the analysis. Secondly, the Pz and Cz channels were not centrally positioned for focal seizures. As a result, excluding data from these channels has minimal impact on the analysis of epileptic EEG signals. Lastly, utilizing EEG data with identical channel configurations facilitated the calculation and comparison of model weight sizes across different methods. This choice is particularly relevant as deep learning models, such as time-series-based CNN, exhibit an increasing number of parameters as the number of channels in EEG expands. There were many variations in the patient recordings, such as ictal onset zones and seizure duration. The dataset utilized in this study consisted of data from six patients, and we included the EEG data of all six patients in our experiment. The scalp EEG signals were bandpass filtered between 1 Hz divided by 1.6 and 70 Hz, and then the 50 Hz electrical utility frequency was removed.

B. Experiment Protocol

We adopted a leave-one(recording)-out cross-validation procedure to evaluate all methods in the experiment. For each patient's seizure recordings, one recording containing interictal and ictal portions was selected as the test set, while the remaining recordings were used as the training set. We then rotated the test set among all recordings until each recording took turns as the test set. MSLBP-HDC and the baseline models were trained individually for each patient.

The EEG data were divided into 0.5-second signal segments as input for all methods, and segments less than 0.5 s were discarded. This decision takes into account the variable duration of seizures present in the dataset. Longer input signal lengths would result in reduced training data of ictal state. By utilizing a 0.5-second signal length as input, we ensured an ample amount of data in the training set, which is crucial for the effectiveness of data-driven machine learning models. Moreover, the model weight size of the baseline models is directly influenced by the input signal length. For wearable devices, it is essential to maintain a small model weight size while ensuring satisfactory detection performance. Leveraging the post-processing module and the 0.5-second signal input not only enhances the accuracy of seizure detection but also mitigates the risk of excessive model weight size. This approach is particularly significant in the context of wearable devices, as it ensures smooth operation without overtaxing the resources. Therefore, all algorithms employed the same post-processing procedure to further improve performance.

In the post-processing procedure, the decision window L_{ps} with a length of 5.5 s was defined. The methods detected seizure onset by post-processing all classification results of scalp EEG segments within the decision window. For the task of detecting epilepsy occurrences, we need to balance detection accuracy and latency when setting the signal length for post-processing. Specifically, setting a smaller signal length for post-processing can effectively reduce the detection latency but may lower the detection accuracy, leading to an increase in false alarm rate and impacting the patient's daily life. Conversely, a larger post-processing signal length can ensure higher detection accuracy but increases the detection latency, potentially depriving the patient of timely assistance and intervention. Therefore, we set the post-processing signal length as 5.5 s to strike a balance between detection accuracy and latency. Moreover, we adopted the majority voting rule to generate the final classification decision. Specifically, if more segments were classified as seizure label, the final decision was deemed as ictal state; otherwise, it was considered interictal state.

C. Parameter Settings of MSLBP-HDC

In this experiment, we set D_W and N_{scale} to 0.5 s and 3, respectively, for multi-scale LBP feature extraction. The values of L^{AW} and L^{msLBP} were [1, 3, 5] and [6, 10, 8], respectively. And the number of LBP codes was [64, 1024, 256] for the three scales in the multi-scale LBP feature, according to the parameter L^{msLBP}. According to Algorithm 1, we can see that the lengths of LBP encoding L_S for three scales were [7, 33, 45], corresponding to short, medium, and long temporal scales in MSLBP-HDC. Previous studies have shown that feature extraction mode with short, medium,

and long temporal scales are useful for EEG analysis [15], [46]. Moreover, setting N_{scale} to 3 is a compromise between accuracy and computational cost. The values of L^{AW} and L^{msLBP} determine the value of L_S, and the determination of L_S is based on the duration of spikes, which are the main features for seizure detection [47]. Since the duration of spikes ranges from 20 to 70 ms [48], feature extraction can be performed on one or more spikes by using encoding lengths of [7, 33, 45] for L_S, corresponding to time duration of [14, 66, 90] ms, thus ensuring the detection accuracy of MSLBP-HDC.

D. Comparison Metrics

Regarding the comparison metrics, we employed specificity, sensitivity, and macroaveraging accuracy to evaluate algorithm performance in epilepsy detection. Specificity is linked to an accurate analysis of interictal periods, and high specificity can effectively reduce false alarms. The calculation of specificity can be written as,

$$Specificity = \frac{\sum_{i=1}^{N_{interictal}} \left(W_i^{interictal} == interictal\right)}{N_{interictal}}, \quad (9)$$

where $N_{interictal}$ is the number of interictal windows in the test set and $W_i^{interictal}$ is the $i-th$ interictal window. Sensitivity measures the ability of the model to detect epilepsy exactly and it can be represented as,

$$Sensitivity = \frac{\sum_{i=1}^{N_{ictal}} \left(W_i^{ictal} == ictal\right)}{N_{ictal}}, \quad (10)$$

where N_{ictal} is the number of ictal windows in the test set and W_i^{ictal} is the $i-th$ ictal window. Macroaveraging accuracy is the average of specificity and sensitivity, and it can be expressed as,

$$Accuracy = \frac{Specificity + Sensitivity}{2}. \quad (11)$$

E. Compared Methods

The compared methods in this experiment include advanced deep learning models, HDC methods, and SVM model. And the HDC methods can be divided into time-series-based, LBP-based and multi-features-based models according to the input. Furthermore, we also investigate the quantized deep learning methods that utilize int8 model weights. Specifically, we employ the Tensorflow Lite Tool to convert the model weights in deep learning models from float32 to int8.

1) TS-LSTM: The time-series-based long short-term memory network (TS-LSTM) processes raw EEG signals and transmits useful information through the gate structure. [18] proposed a TS-LSTM architecture that achieves good performance in seizure detection.

2) TS-CNN: The time-series-based convolutional neural network (TS-CNN) applies a convolutional structure to extract task-related features from EEG time series. In [15], the TS-CNN architecture design adopts the multi-scale convolutional layer and length-one convolution. It shows high accuracy not only for epileptic EEG but also for other EEG-based brain-computer interface paradigms.

3) LBP-CNN: The LBP-based convolutional neural network (LBP-CNN) combines traditional LBP features and convolutional structure to analyze epileptic EEG data. LBP-CNN in [16] can accurately classify different brain states from EEG signals.

4) LBP-LSTM: The LBP-based long short-term memory network (LBP-LSTM) feeds the extracted conventional LBP features to the LSTM network. We consider the model architecture in [19] and tune its hyperparameters for epilepsy detection.

5) TS-HDC: The time-series-based hyperdimensional computing method (TS-HDC) utilizes the continuous item memory to map the quantized amplitude levels to the hypervectors. TS-HDC, as presented in [36], can be employed for seizure onset detection.

6) LBP-HDC: The LBP-based hyperdimensional computing method (LBP-HDC) in [39] encodes the traditional LBP features to hypervectors and conducts analysis in hyperdimensional space. It is also the state-of-the-art HDC method for classifying ictal and interictal states in iEEG.

7) MF-HDC: The multi-features-based hyperdimensional computing method (MF-HDC) incorporates features from mean amplitude, power spectral density, and line length [49] for epileptic EEG analysis. We utilize the $Ch \times F \times V$ architecture of MF-HDC proposed in [34] for performance comparison.

8) LBP-SVM: The LBP-based support vector machine method (LBP-SVM) employs traditional LBP features as input for the SVM model. In [10], the authors developed the LBP-SVM approach for epileptic EEG analysis and achieved commendable accuracy performance.

IV. Results

A. Classification Results

TABLE I illustrates the mean specificity, sensitivity, and accuracy across all patients for MSLBP-HDC and the other compared methods, where SEM denotes the standard error of the mean. From the table, it is evident that MSLBP-HDC attains the highest specificity (96.18%) compared to all other algorithms. Additionally, LBP-based approaches such as LBP-HDC, LBP-SVM, and LBP-based deep learning models demonstrate superior specificity when compared to TS-based algorithms, including TS-HDC and TS-based deep learning methods. Due to the omission of temporal dynamic features during feature extraction, MF-HDC exhibits the lowest specificity compared to all other methods. High specificity, is necessary for the algorithm to be deployed in the real environment, as it can effectively reduce false alarm rate and avoid corresponding patient anxiety [50]. In the experiment, MSLBP-HDC also achieves the highest average accuracy

TABLE I: Average specificity, sensitivity, and accuracy across all patients for MSLBP-HDC and the existing methods. SEM denotes the standard error of the mean.

Work	Model	Specificity ± SEM (%)	Sensitivity ± SEM (%)	Accuracy ± SEM (%)
Our work	MSLBP-HDC	**96.18 ± 1.36**	88.76 ± 6.30	**92.47 ± 3.01**
Ccalicskan et al, 2022 [18]	TS-LSTM	78.26 ± 7.79	57.90 ± 12.32	68.08 ± 7.31
Du et al, 2022 [15]	TS-CNN	74.91 ± 6.97	**89.48 ± 7.33**	82.20 ± 5.84
Dhar et al, 2022 [16]	LBP-CNN	95.40 ± 1.72	82.19 ± 7.09	88.79 ± 3.41
Shekokar et al, 2021 [19]	LBP-LSTM	93.66 ± 3.32	88.95 ± 7.21	91.31 ± 3.77
Pale et al, 2021 [36]	TS-HDC	70.10 ± 4.28	67.85 ± 5.69	68.97 ± 3.89
Burrello et al, 2019 [39]	LBP-HDC	92.71 ± 1.93	85.49 ± 5.71	89.10 ± 2.83
Pale et al, 2022 [34]	MF-HDC	53.91 ± 10.89	79.46 ± 8.32	66.68 ± 8.24
Jaiswal et al, 2017 [10]	LBP-SVM	92.71 ± 3.02	83.77 ± 7.82	88.24 ± 3.91
Ccalicskan et al, 2022 [18]	Quantized TS-LSTM	78.26 ± 7.79	57.95 ± 12.28	68.10 ± 7.20
Du et al, 2022 [15]	Quantized TS-CNN	74.91 ± 6.97	88.09 ± 8.71	81.50 ± 6.46
Dhar et al, 2022 [16]	Quantized LBP-CNN	95.23 ± 1.72	82.34 ± 7.13	88.78 ± 3.40
Shekokar et al, 2021 [19]	Quantized LBP-LSTM	93.84 ± 3.15	88.80 ± 7.19	91.32 ± 3.74

(92.47%). When compared to quantized LBP-LSTM, which has the best accuracy (91.32%) among all deep learning models, MSLBP-HDC attains better accuracy while having a smaller model weight size, as shown in Fig. 2. MSLBP-HDC only needs one training iteration to achieve such high performance, while the training iterations of deep learning models were set to 100 in the experiment to get a satisfactory performance. Additionally, we can observe that the LBP-based methods outperform time-series-based methods and MF-HDC in terms of accuracy, demonstrating the effectiveness of LBP features in seizure detection. For the mean sensitivity, the time-series-based method TS-CNN performs best (89.48%). It should be noted that both MSLBP-HDC and TS-CNN adopt the idea of multi-scale feature extraction for epileptic EEG analysis. MSLBP-HDC achieves better specificity and accuracy than TS-CNN, and we will improve the sensitivity performance of MSLBP-HDC later to make it more practical.

Fig. 2 shows the model weight size versus macroaveraging accuracy for all algorithms. We can clearly see that MSLBP-HDC outperforms other classifiers in model weight size and accuracy, demonstrating the practicality of our proposed method for epilepsy detection on wearable devices. In comparison to deep learning models and SVM, HDC models achieve the smallest model weight size, as they only need to store the class hypervectors and the random seed [51], [39]. Additionally, the item memory in HDC models can be easily reconstructed from the random seed using cellular automaton [42]. For our proposed MSLBP-HDC, we set the dimension of the hypervector to be 3,000 and N_{scale} to be 3. Therefore, the model weight size of MSLBP-HDC can be calculated as the sum of the weight of class hypervectors (18 kbits) and the weight of the random seed (64 bits). It is evident that the quantized deep learning models achieve similar accuracy to their non-quantized counterparts but with smaller model weight size. Due to the simplicity of LBP features and the translation invariance of the convolutional structure, quantized LBP-CNN has the smallest model weight size among all deep learning models (approximately two times larger than MSLBP-HDC). Although quantized LBP-LSTM achieves the highest accuracy in all deep learning methods, its larger model weight size, about 450 times larger than MSLBP-HDC, limits its implementation on wearable devices. The binary weights and operations in MSLBP-HDC are hardware-friendly. This is significant for the long-term monitoring of epilepsy patients on portable devices. In contrast, deep learning models require floating-point or integer operations, which pose higher hardware requirements and make their application more challenging. Additionally, it can be observed that time series-based methods, including TS-CNN, TS-LSTM, and TS-HDC, exhibit poor performance due to the disparity in features between amplitudes in time series and LBP codes. Moreover, MF-HDC demonstrates lower accuracy in comparison to the TS-HDC and LBP-HDC methods, despite having the same model weight size.

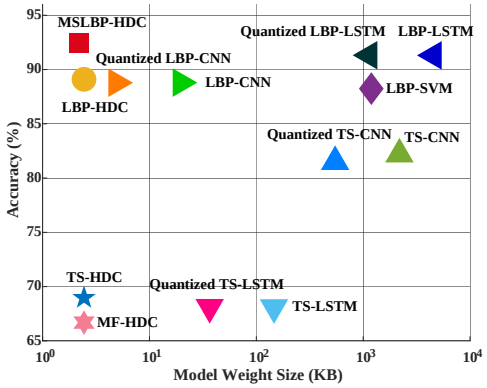

Fig. 2: The model weight size versus macroaveraging accuracy for MSLBP-HDC and the other compared algorithms.

The mean specificity, sensitivity, and accuracy of MSLBP-HDC and compared methods for different seizure types are shown in TABLE II. To assess the analytical performance of various methods on different types of epileptic EEG data, we calculate the average performance by aggregating the specificity, sensitivity, and accuracy of MSLBP-HDC and baseline models for patients with the same seizure type. It can be observed that MSLBP-HDC achieves the highest specificity among all models for all seizure types, which is consistent with the observations in TABLE I. The high specificity of MSLBP-HDC ensures a low probability of false detection in the applications. From the table, it is evident that our proposed method achieves the best performance across all three metrics

TABLE II: Mean specificity (SPE), sensitivity (SEN), and accuracy (ACC) of MSLBP-HDC compared to other methods on different seizure types, including complex partial seizure, electrographic seizure, and video-detected seizure with no visual change over EEG.

	Complex Partial Seizure			Electrographic Seizure			Video-Detected Seizure		
	Spe (%)	Sen (%)	Acc (%)	Spe (%)	Sen (%)	Acc (%)	Spe (%)	Sen (%)	Acc (%)
MSLBP-HDC	**95.05**	**86.93**	**90.99**	**96.88**	84.83	90.85	**100.00**	**100.00**	**100.00**
TS-LSTM	84.38	51.22	67.80	50.00	53.64	51.82	82.03	88.89	85.46
TS-CNN	79.56	84.23	81.89	50.00	**100.00**	75.00	81.25	**100.00**	90.63
LBP-CNN	94.66	76.61	85.63	93.75	92.95	93.35	**100.00**	93.75	96.88
LBP-LSTM	91.28	85.13	88.20	**96.88**	93.18	**95.03**	**100.00**	**100.00**	**100.00**
TS-HDC	69.40	64.48	66.94	59.38	60.28	59.83	83.59	88.89	86.24
LBP-HDC	91.80	84.58	88.19	89.06	80.91	84.99	**100.00**	93.75	96.88
MF-HDC	58.20	73.99	66.10	20.31	86.36	53.34	70.31	94.44	82.38
LBP-SVM	90.63	81.90	86.26	93.75	81.31	87.53	**100.00**	93.75	96.88
Quantized TS-LSTM	84.38	50.84	67.61	50.00	55.45	52.73	82.03	88.89	85.46
Quantized TS-CNN	79.56	82.14	80.85	50.00	**100.00**	75.00	81.25	**100.00**	90.63
Quantized LBP-CNN	94.79	76.61	85.70	92.19	93.86	93.03	**100.00**	93.75	96.88
Quantized LBP-LSTM	91.54	85.13	88.33	**96.88**	92.27	94.57	**100.00**	**100.00**	**100.00**

in the analysis of complex partial seizures. Regarding EEG signals with electrographic seizures, MSLBP-HDC, LBP-LSTM, and quantized LBP-LSTM demonstrate the highest specificity. However, it can be observed that time-series-based models (TS-CNN, TS-LSTM, and TS-HDC) and MF-HDC exhibit low specificity in the analysis of electrographic seizures. TS-CNN and its quantized counterpart exhibit the best sensitivity, while LBP-LSTM shows the highest accuracy among all the methods. In the analysis of video-detected seizures without visual changes over EEG, MSLBP-HDC, LBP-SVM, LBP-HDC, LBP-based deep learning models and their quantized counterparts achieve the highest sensitivity, demonstrating the usefulness of LBP features in detecting this type of seizure. MSLBP-HDC, TS-CNN, and their quantized models, as well as LBP-LSTM and its quantized model, display the best sensitivity performance. Furthermore, in terms of accuracy, it is apparent that LBP-based methods outperform time-series-based methods, with MSLBP-HDC, LBP-LSTM, and quantized LBP-LSTM achieving the highest accuracy performance.

B. Few-Shot Learning Performance

Machine learning methods are capable of achieving satisfactory accuracy with enough training data. However, in real-world situations, acquiring clean and reliable scalp EEG signals can be challenging in noisy environments or when the patient has excessive movement or muscle activity [15]. Uncertainty about seizures also makes annotated data harder to come by [39]. Therefore, few-shot learning performance is important for machine learning methods to conduct seizure detection with small training data.

In the few-shot learning experiment, we employed a leave-one(recording)-out cross-validation procedure. For each iteration, a complete recording of a patient, encompassing both interictal and ictal portions, was selected as the test set, while the remaining recordings were considered as candidates for the training set. Subsequently, we randomly sampled 1% of data from the interictal and ictal portions of the candidate training set for the few-shot learning experiment. Specifically, we initially selected a recording randomly from the candidate training set. If the number of data points within the interictal and ictal portions of this recording satisfied the requirement, i.e., greater than or equal to 1% of the overall candidate training set, we utilized the data from this recording as the training set for the few-shot learning experiment. In cases where the quantity fell short of the 1% threshold, we continued to select subsequent recordings randomly until the desired quantity was met. On average, the number of data points within the training set for the few-shot learning experiment was 21.08 across all six patients in the dataset.

Fig. 3 shows the performance of MSLBP-HDC, MSLBP-LSTM, MSLBP-CNN, and MSLBP-SVM with only 1% of the available training data in the dataset, where Fig. 3(a) illustrates the average accuracy across all patients, and Fig. 3(b) depicts the accuracy for six patients. It should be noted that MSLBP-HDC, deep learning models, and SVM adopt the same multi-scale LBP features as input for a fair comparison. As shown in Fig. 3(a), when using small training data, MSLBP-HDC maintains high accuracy performance, while the accuracy of CNN and LSTM is relatively low, demonstrating the practicability of our proposed method in epilepsy detection tasks on scalp EEG. MSLBP-SVM achieves the second-highest accuracy performance among all the methods. However, the model weight size of SVM is larger than that of MSLBP-HDC, as shown in Fig. 2, which limits its implementation in real scenarios. Furthermore, MSLBP-HDC, MSLBP-LSTM, and MSLBP-SVM can enhance accuracy by increasing the post-processing signal length, whereas the accuracy of MSLBP-CNN remains nearly unchanged. In Fig. 3(b), MSLBP-HDC achieves the best accuracy performance in three out of six patients (patients 1, 4, and 6), illustrating the robustness of our approach in learning seizure-related features from a limited amount of data. In the case of patient 6, our analysis reveals that MSLBP-HDC, MSLBP-SVM, and MSLBP-CNN exhibit remarkably similar high-performance levels. However, MSLBP-LSTM demonstrates relatively lower accuracy in comparison. Our proposed MSLBP-HDC achieves almost 100% accuracy for patient 4 using only 1% of the training data. For patient 2, the performance gap between MSLBP-HDC and LSTM gradually narrows as L_{ps} increases in the post-processing module. For patients 3 and 5, MSLBP-CNN and

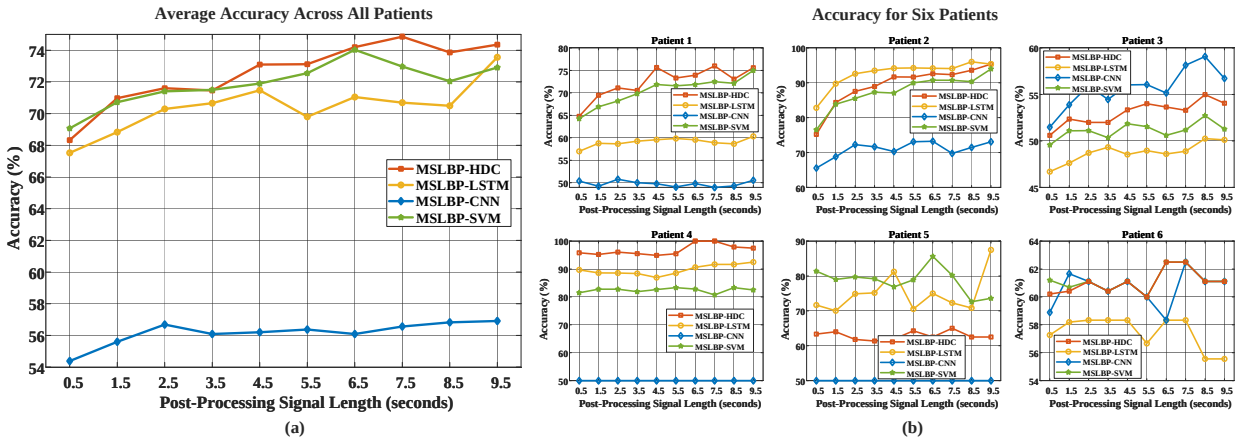

Fig. 3: Few-shot learning performance of MSLBP-HDC, deep neural networks and SVM with multi-scale LBP features using 1% of the training data: Average accuracy across all patients (a) and accuracy for six patients (b) with different post-processing signal lengths.

MSLBP-SVM are the best-performing models, respectively.

In the few-shot learning experiment, only 1% of the original training data was used to train the model. It should be noted that EEG signals with weak amplitudes are easily influenced by noise and artifacts. In such cases, anomalous samples that are affected by noise and artifacts may prevent the model from accurately capturing essential features related to epilepsy detection in EEG data, resulting in unstable feature extraction and overfitting on anomalous data in the model training stage. Consequently, insufficient training samples can lead to poor generalization performance of models on certain subjects, particularly for data-driven deep learning models such as MSLBP-CNN. As evident from Fig. 3(b), all methods exhibit performance variations across different patients. Unlike our proposed MSLBP-HDC which achieves high accuracy performance across multiple subjects, MSLBP-CNN fails to learn useful features related to epileptic EEG signals for patients 1, 4, and 5, resulting in an accuracy of only around 50% on these three subjects. Moreover, the accuracy of MSLBP-CNN does not improve with an increase in the post-processing signal length of these three patients due to its weak feature extraction ability. The poor performance of MSLBP-CNN on these three patients contributes to its low average accuracy across all patients in Fig. 3(a). It can be clearly seen from Fig. 3(a) that the average accuracy remains almost unchanged as the post-processing signal length increases. In contrast, for patients like patient 2, where MSLBP-CNN successfully learns relevant features, the accuracy improves from 65.54% to 73.08% as the post-processing signal length increases. In summary, the results depicted in Fig. 3 demonstrate the robustness of MSLBP-HDC in monitoring different epilepsy patients with limited annotated data. Improving the few-shot learning performance of MSLBP-HDC further is one of our future works, which can enhance the practicality of our method.

C. Feature Explainability Analysis

Fig. 4 illustrates the feature relevance topographies for patients with partial seizure locations during the ictal and interictal phases, namely patients 1, 2, 5, and 6. It is evident from the figure that there are significant differences in the feature relevance topographies between seizure and non-seizure states. Specifically, the features in MSLBP-HDC during the ictal phase, especially the hypervectors at the partial seizure sites, exhibit a large difference from the features during the interictal phase, i.e., a higher normalized Hamming distance. On the other hand, the hypervectors from EEG signals during the interictal phase do not differ significantly from each other.

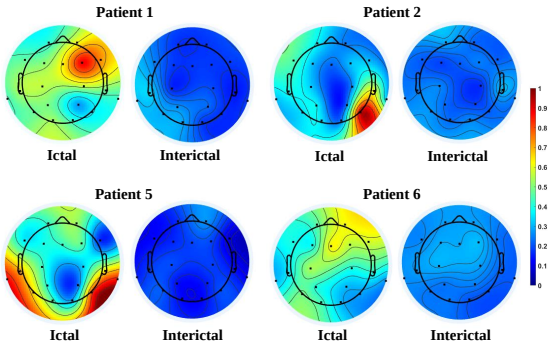

Fig. 4: The feature relevance topographies for patients with partial seizure locations during the ictal and interictal phases, where the color bar indicates the normalized Hamming distance.

From the results of patient 1, it can be seen that the largest normalized Hamming distance between hypervectors appears near the right anterior temporal and right frontal lobes, implying that the useful features are concentrated at this location for MSLBP-HDC to conduct seizure detection. This finding is consistent with the doctor's diagnosis in the dataset: the focal point of patient 1 was close to the right anterior temporal and right frontal lobes [45]. Similar results are observed for patients 2, 5, and 6. The primary seizure sites for these patients are the right posterior temporal lobe, left middle temporal lobe, and right frontal lobe, respectively, which are consistent with the doctor's diagnosis. Compared to statistical analysis, which necessitates a large sample size

to obtain localization results for the ictogenic brain region, rating the feature importance (Hamming distance) of channels with MSLBP-HDC can provide diagnostic results similar to those of doctors using only a 20-second signal segment. This approach is more appropriate for localizing the ictogenic brain region since seizures have a limited duration [52]. In such cases, statistical analysis may not yield significant localization results. Overall, MSLBP-HDC is able to identify the seizure location in a short period of time for different patients, demonstrating its reliability and generalizability.

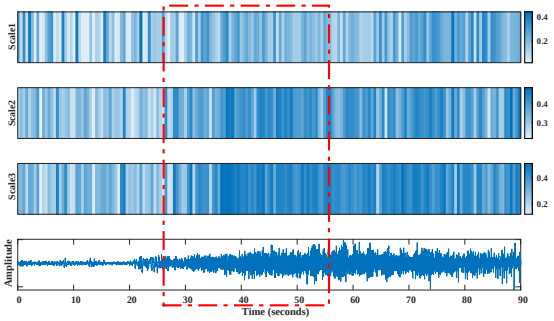

Fig. 5: The feature relevance between Epileptic EEG signals and hypervectors of MSLBP-HDC at different temporal scales in the time domain, where the colour bars denote the normalized Hamming distance. Scale 1, 2, and 3 represent short, medium, and long temporal scales in MSLBP-HDC, respectively.

The feature relevance between epileptic EEG and hypervectors of MSLBP-HDC at different temporal scales in the time domain is shown in Fig. 5, which is generated from the test set in one randomly chosen fold of the dataset. The feature difference is obtained by comparing the normalized Hamming distance of the hypervectors with seizure and non-seizure labels at different times. It can be clearly seen that for hypervectors of different temporal scales, when epilepsy occurs, the normalized Hamming distance from the hypervector without seizure becomes larger, indicating that MSLBP-HDC extracts epilepsy-related features to encode hypervectors and conduct detection. Additionally, the hypervectors at long temporal scale (scale 3) exhibit the more obvious feature differences for seizure onset, since long-scale feature extraction is more resistant to the interference of noise and artifacts. This verifies the necessity of long-scale LBP-feature extraction in our proposed method.

Fig. 6 depicts the t-SNE feature visualization of MSLBP-HDC's hypervectors at different temporal scales for video-detected seizures with no visual change over EEG. It should be noted that the test set is a randomly selected recording from the epileptic EEG dataset. Although there are no obvious changes in the scalp EEG time series, the feature distribution of hypervectors reflects distinguishability between the interictal and ictal portions at different temporal scales, demonstrating the effectiveness of MSLBP-HDC for analyzing this seizure type.

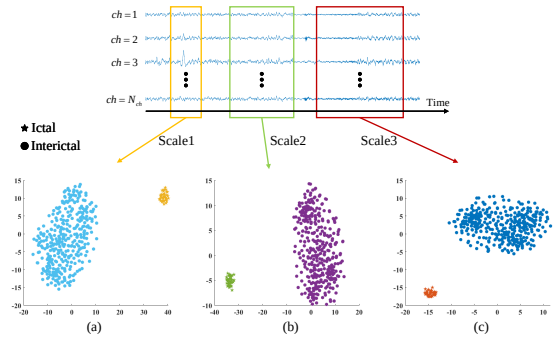

Fig. 6: The t-SNE projections of MSLBP-HDC's hypervectors at different temporal scales for video-detected seizure with no visual change over EEG, where scale 1, 2, and 3 denote short, medium and long temporal scales in MSLBP-HDC, respectively.

D. Embedded Implementation Analysis

In this subsection, we conduct a comprehensive analysis of the embedded deployment of MSLBP-HDC. One of the major challenges in this deployment arises from the significant data transfers involved in the calculation of hypervectors within the HDC model [53]. To address this issue, a promising approach to meet the requirements for advanced low-power, high-speed computing platforms is to leverage next-generation memristive devices to perform HDC. Among the various non-volatile memory (NVM) technologies, Resistive Random Access Memory (RRAM) [54] exhibits multi-state programmability and promising compute-in-memory (CIM) potential in the next-generation HDC area. Efficient CIM is able to minimize dramatically the need for extensive data movement, leading to improved energy efficiency in the implementation of MSLBP-HDC. In our work, we utilize the extensively modified DNN+NeuroSim integration framework [55] to evaluate the performance of RRAM in the context of MSLBP-HDC. This framework offers flexible and hierarchical CIM array design options, ranging from device-level to circuit-level and up to algorithm-level, providing us with highly accurate prediction outcomes [56].

Table III provides a comprehensive overview of the energy efficiency and latency of embedded implementation of MSLBP-HDC, along with comparisons to other existing works in the field of epileptic EEG analysis. The results clearly demonstrate that MSLBP-HDC achieves the highest energy efficiency (0.14 µJ/class) due to its binary model architecture and the CIM capability of RRAM hardware. In contrast, Li *et al.* achieved an energy efficiency of 8.12 µJ/class [57], and Lammie *et al.* achieved 18.7 µJ/class by employing CNN on RRAM [58]. These results demonstrate that the utilization of CNN with RRAM technology requires higher energy for epileptic EEG analysis compared to the HDC model. Furthermore, the deployment of the HDC model within a microcontroller unit (MCU) consumed significantly more energy (18.5 µJ/class) compared with MSLBP-HDC on RRAM [50]. Ai *et al.* achieved an energy efficiency of 0.15 µJ/class by utilizing a CNN hardware deployment with 65-nm complementary

TABLE III: Energy efficiency and latency about embedded implementations of MSLBP-HDC and other existing works for epileptic EEG analysis.

Work	Method	Technology	Energy Efficiency	Latency	Simulation/Measurement
Our work	Hyperdimensional Computing	RRAM	**0.14** µJ/class	231.91 µs	Simulation
Li et al, 2022 [57]	Convolutional Neural Network	RRAM	8.12 µJ/class	**1.13** µs	Simulation
Lammie et al, 2022 [58]	Convolutional Neural Network	RRAM	18.7 µJ/class	11 µs	Simulation
Burrello et al, 2021 [50]	Hyperdimensional Computing	MCU	18.5 µJ/class	-	Measurement
Zhan et al, 2019 [59]	Support Vector Machine	FPGA	-	10.2 µs	Measurement
Wen et al, 2022 [60]	Support Vector Machine	65-nm CMOS	2.23 µJ/class	-	Simulation
Ai et al, 2023 [61]	Convolutional Neural Network	65-nm CMOS	0.15 µJ/class	3.29 ms	Simulation
Su et al, 2022 [62]	Support Vector Machine	130-nm CMOS	1.28 µJ/class	-	Measurement
Cheng et al, 2018 [63]	Ridge Regression	180-nm CMOS	62.5 µJ/class	-	Measurement

metal-oxide-semiconductor (CMOS) technology, surpassing the hardware implementations of SVM [60], [62] and ridge regression [63] for epileptic EEG analysis.

In terms of latency, MSLBP-HDC achieves a delay of 231.91 µs on RRAM, outperforming the 3.29 ms achieved by CNN in a 65-nm CMOS hardware deployment [61]. It is worth noting that the achieved latency of 231.91 µs, equivalent to 4.31 kHz, in our scheme is more than sufficient for real-time monitoring of seizure onset in wearable devices. Zhan *et al.* achieved a latency of 10.2 µs by deploying SVM using field-programmable gate arrays (FPGA) [59], while Lammie *et al.* obtained 11 µs using CNN on RRAM [58]. Significantly, Li *et al.* achieved the minimal latency (1.13 µs) using CNN on RRAM [57]. Benefiting from the excellent CIM capability of RRAM, the embedded deployment of models on RRAM achieves optimal energy efficiency (MSLBP-HDC) and latency (CNN) among all the compared works. Notably, our proposed method on RRAM achieves the best energy efficiency for epilepsy detection. Given the importance of energy consumption in long-term monitoring applications, this emphasizes the effectiveness of MSLBP-HDC and RRAM for wearable EEG devices.

Fig. 7 provides a breakdown of the energy usage and latency for the embedded implementation of MSLBP-HDC in a typical classification scenario. Regarding energy usage, the ADC and accumulation circuits collectively contribute to 3.65% and 3.71%, respectively, while other peripherals such as decoders, mux, switch matrix, and buffers account for 92.64% of the overall energy consumption. A similar distribution is observed in the latency breakdown, where the ADC and accumulation circuits contribute to 2.20% and 4.93% of the total latency, respectively, and other peripherals account for 92.87% of the overall latency.

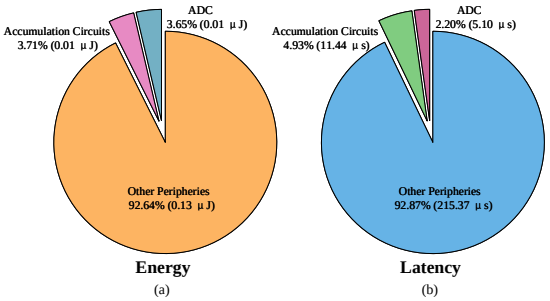

Fig. 7: Energy usage (a) and latency (b) breakdown about embedded implementation of MSLBP-HDC for a typical classification.

V. Ablation Studies

In this section, we present ablation studies to demonstrate the effectiveness of each component in our proposed MSLBP-HDC model. Unlike the traditional LBP encoding that analyzes EEG signals only at short temporal scales, the designed multi-scale LBP codes contain features at three temporal scales: short, medium, and long. To evaluate the efficacy of the newly added medium and long scales, we conduct a comparison between MSLBP-HDC and three existing solutions, namely TS-HDC, LBP-HDC, and MF-HDC, using identical bit-length conditions. LBP-HDC solely employs features extracted from the short temporal scale, whereas TS-HDC utilizes raw amplitude features of EEG signals. And MF-HDC adopts the features from both amplitude and power spectral density for seizure detection. In addition, to assess the effectiveness of using HDC for encoding multi-scale LBP features, we compare the performance gain of HDC with deep learning models, including CNN and LSTM, when using multi-scale LBP features. The gain is computed by comparing it with the performance of traditional LBP-based models.

A. Comparison with Existing HDC Methods

1) Performance comparison under different hypervector settings: To explore the performance of the MSLBP-HDC method further, we compare its mean specificity, sensitivity, and accuracy with TS-HDC, LBP-HDC, and MF-HDC methods, using hypervectors of the same bit length in the HDC models. As shown in TABLE IV, MSLBP-HDC outperforms other HDC methods under different hypervector settings. MSLBP-HDC is capable of analyzing spikes with varying durations using multi-scale features, whereas LBP-HDC, with only a single short-scale feature, TS-HDC, with raw amplitude features, and MF-HDC, with the overall characteristic features of EEG time series, cannot achieve this. Furthermore, it is evident that LBP-based HDC models outperform TS-based and MF-based HDC models under different hypervector settings, demonstrating the effectiveness of LBP features in seizure detection.

Increasing the bit length in the HDC model significantly improves the performance of MSLBP-HDC and TS-HDC, while no similar improvement is observed for LBP-HDC and

TABLE IV: Performance comparison of MSLBP-HDC, TS-HDC, LBP-HDC, and MF-HDC methods using hypervectors of equal bit length in the HDC models, where Spe, Sen, and Acc denote specificity, sensitivity, and accuracy, respectively.

	$D = 3000$			$D = 6000$			$D = 9000$		
	Spe (%)	Sen (%)	Acc (%)	Spe (%)	Sen (%)	Acc (%)	Spe (%)	Sen (%)	Acc (%)
MSLBP-HDC	94.36	88.49	91.43	95.23	88.47	91.85	96.18	88.76	92.47
TS-HDC	67.62	57.71	62.67	68.71	67.98	68.34	67.71	68.56	68.13
LBP-HDC	93.32	85.36	89.34	92.53	86.00	89.27	93.06	85.83	89.44
MF-HDC	58.33	77.72	68.03	54.60	80.56	67.58	54.34	78.49	66.42

MF-HDC. When using 3000 bits in the hypervectors, the accuracy of MSLBP-HDC reaches 91.43%, compared to 89.34% for LBP-HDC, 62.67% for TS-HDC, and 68.03% for MF-HDC. Applying 9000 bits in the HDC model further improves the accuracy of MSLBP-HDC to 92.47%, while LBP-HDC achieves 89.44%, TS-HDC achieves 68.13%, and MF-HDC achieves only 66.42%. TS-HDC achieves the largest sensitivity gain when increasing the bit length in the hypervectors. The sensitivity of TS-HDC increase from 57.71% to 68.56% when HDC uses 3000 bits to 9000 bits in the hypervector settings. Moreover, when using 9000 bits in hypervectors, the sensitivity of MSLBP-HDC is 88.76%, while that of LBP-HDC is 85.83%, MF-HDC achieves 78.49%, and TS-HDC achieves only 68.56%. The difference in sensitivity highlights the practicality of our method in seizure detection. In practical applications, we set $D = 9,000$ in the MSLBP-HDC to balance the model weight size and accuracy. When performing 24-hour real-time epilepsy detection using wearable devices, a high model weight size would increase the computational burden and slow down the operation in embedded systems. Therefore, while ensuring high accuracy, it is crucial to minimize the model weight size as much as possible.

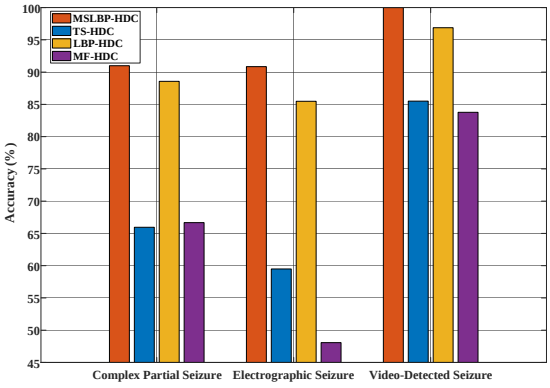

Fig. 8: Accuracy Performance of MSLBP-HDC and other existing HDC methods for the analysis of different seizure types, under the condition of using 9000 bits hypervectors in the HDC models.

Fig. 8 presents the accuracy performance of MSLBP-HDC, TS-HDC, and LBP-HDC methods for the analysis of different seizure types, under the condition of using 9000 bits hypervectors in the HDC models. As depicted in the figure, MSLBP-HDC demonstrates superior performance compared to other HDC models when considering various seizure types with the same bit length in the hypervectors. Additionally, all HDC methods exhibit improved accuracy in the analysis of video-detected seizures when compared to complex partial seizures and electrographic seizures. This finding suggests that the HDC model excels in analyzing epileptic EEG signals of this specific type. Notably, for complex partial seizures and electrographic seizures, both MSLBP-HDC and LBP-HDC exhibit higher accuracy performance than TS-HDC and MF-HDC.

2) Performance comparison under different initialization seed settings in the item memory: Furthermore, we investigate the impact of different initialization seeds in the item memory on the performance of HDC methods. Fig. 9 depicts the distributions of specificity, sensitivity, and accuracy of MSLBP-HDC, TS-HDC, LBP-HDC, and MF-HDC with different initialization seeds in the item memory. The HDC methods were trained using the leave-one(recording)-out cross-validation procedure and then evaluated for their performance. All HDC methods were trained five times with different initialization seed settings in the item memory. From the figure, it is evident that MSLBP-HDC exhibits minimal fluctuations in performance due to the adopted ensemble structure in the model. MSLBP-HDC achieves the highest performance in terms of specificity, sensitivity, and accuracy compared to TS-HDC, LBP-HDC, and MF-HDC methods. On the other hand, TS-HDC shows the largest fluctuations with different initialization seeds in the item memory. Such large performance fluctuations increase resource consumption during the training process to find the suitable seed settings, which is not conducive to the practical implementation of patient epilepsy detection.

3) Advantages Over LBP-HDC: Compared with LBP-HDC, our proposed MSLBP-HDC showcases several notable advancements in input feature, model architecture, and detection performance. MSLBP feature takes into account the scalp EEG's susceptibility to noise interference and the duration of spikes, which are the distinctive characteristics of epileptic EEG. As a result, MSLBP is able to extract dynamic features at various time resolutions to capture abnormal cortical oscillations, which traditional LBP feature cannot achieve. Regarding the model architecture, MSLBP-HDC has specific adaptations to the HDC model to accommodate MSLBP features. Unlike traditional HDC models that use hypervectors with a high dimensionality of 10,000, we designed individual HDC models with a relatively lower dimensionality of 3,000 in hypervectors for each scale feature within the MSLBP, thus optimizing the model weight size. Additionally, we employed a model ensemble structure to integrate the analysis results from these sub-HDC models. In terms of model performance, MSLBP-HDC demonstrates superior detection performance compared to the

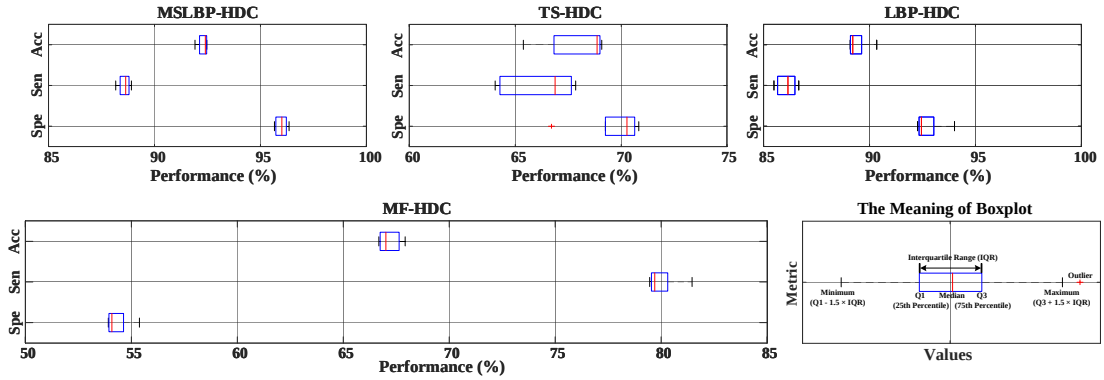

Fig. 9: The distributions of average specificity (Spe), sensitivity (Sen), and accuracy (Acc) of MSLBP-HDC, TS-HDC, LBP-HDC, and MF-HDC with different initialization seeds in the item memory. All HDC methods were trained using the leave-one(recording)-out cross-validation procedure five times with different initialization seed settings in the item memory.

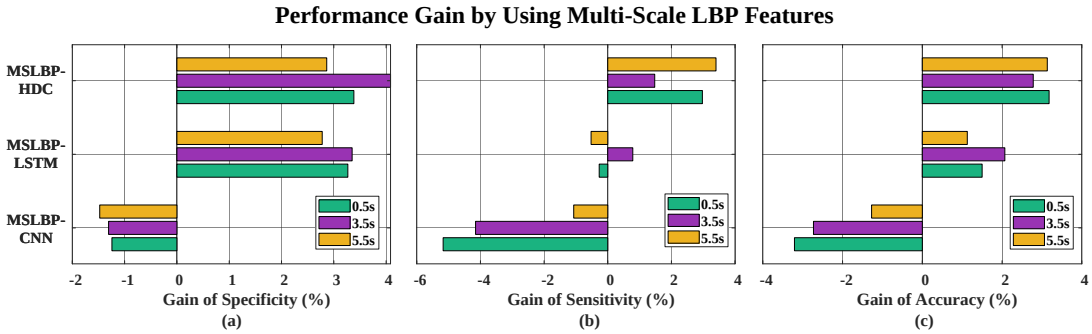

Fig. 10: The performance gain of HDC and deep learning models by using multi-scale LBP features with post-processing signal lengths of 0.5s, 3.5s, and 5.5s.

LBP-HDC method. Our proposed method achieves higher detection performance while significantly reducing the model weight size. And MSLBP-HDC consistently outperforms LBP-HDC when analyzing different seizure types. In addition, MSLBP-HDC demonstrates enhanced stability and accuracy in seizure detection across different random initializations of the item memory.

B. Performance Improvement with Multi-Scale LBP Features

Fig. 10 illustrates the performance improvement of HDC and deep learning models by employing the proposed multi-scale LBP features, compared with the models using traditional short-scale LBP features. It should be noted that all methods adopt the same post-processing procedure, and the lengths of decision window L_{ps} are 0.5 s, 3.5 s, and 5.5 s in this experiment. We can see from the figure that the sensitivity and accuracy of HDC improve the most for the different L_{ps} settings, indicating that the designed multi-scale LBP features are more suitable for HDC to analyze epileptic EEG signals. With the 5.5 s signal segments as input in the post-processing module, the HDC model achieves 2.86%, 3.40%, and 3.13% gains in specificity, sensitivity, and accuracy, respectively. It is significant for HDC to enhance the sensitivity performance because the existing LBP-HDC model is weak in this metric, as shown in TABLE I.

Furthermore, the LSTM model also obtains performance enhancement by applying multi-scale LBP features, especially for the specificity metric. And the improvements in accuracy are 1.50%, 2.07%, and 1.13%, respectively, as the L_{ps} increases. In contrast, the CNN method has no performance gain but a performance loss with multi-scale LBP features. For example, it has a 1.31%, 4.15%, and 2.73% loss in specificity, sensitivity, and accuracy when the 3.5 s signal segments are used as the input of the post-processing module. Investigating the reason for the performance loss and improving the generalizability of multi-scale LBP features for different methods are some of our future works.

VI. Conclusion

In this study, we proposed an HDC model named MSLBP-HDC to enhance the epilepsy detection performance of scalp EEG on wearable devices. The designed multi-scale LBP codes can integrate multi-scale information to capture the dynamic features of scalp EEG signals. In addition, we adopted a model ensemble to further improve the accuracy and robustness of MSLBP-HDC. In this way, MSLBP-HDC can extract useful features of scalp EEG from different temporal scales to overcome the influence of noise and improve the detection performance for different seizure types, especially in small datasets. We evaluated our method on an epileptic EEG dataset acquired in real clinical scenarios, and the results demonstrate

that MSLBP-HDC achieves better detection performance with the smallest model weight size compared to other methods. Moreover, the feature explainability analysis illustrates that our model is able to extract abnormal cortical oscillations rather than noise or artifacts for seizure detection.

However, our proposed method has certain limitations. Firstly, there is room for further improvement in the sensitivity of MSLBP-HDC. Secondly, the detection performance of MSLBP-HDC on electrographic seizures is relatively lower compared to its analysis on other seizure types. In future work, we aim to improve the performance of MSLBP-HDC, with a specific focus on enhancing its sensitivity, detection performance for electrographic seizures, and few-shot learning capability. Additionally, we plan to evaluate the usefulness of MSLBP feature on more machine learning models.

REFERENCES

[1] R. Bandopadhyay, T. Singh, M. M. Ghoneim, S. Alshehri, E. Angelopoulou, Y. N. Paudel, C. Piperi, J. Ahmad, N. A. Alhakamy, M. A. Alfaleh *et al.*, "Recent developments in diagnosis of epilepsy: scope of microrna and technological advancements," *Biology*, vol. 10, no. 11, p. 1097, 2021.

[2] A. Bernasconi, "Connectome-based models of the epileptogenic network: a step towards epileptomics?" *Brain*, vol. 140, no. 10, pp. 2525–2527, 2017.

[3] E. Beghi, "The epidemiology of epilepsy," *Neuroepidemiology*, vol. 54, no. 2, pp. 185–191, 2020.

[4] R. D. Thijs, R. Surges, T. J. O'Brien, and J. W. Sander, "Epilepsy in adults," *The Lancet*, vol. 393, no. 10172, pp. 689–701, 2019.

[5] R. J. Staba, M. Stead, and G. A. Worrell, "Electrophysiological biomarkers of epilepsy," *Neurotherapeutics*, vol. 11, pp. 334–346, 2014.

[6] A. K. Idrees, S. K. Idrees, R. Couturier, and T. Ali-Yahiya, "An edge-fog computing-enabled lossless eeg data compression with epileptic seizure detection in iomt networks," *IEEE Internet of Things Journal*, vol. 9, no. 15, pp. 13 327–13 337, 2022.

[7] R. Singh, T. Ahmed, A. K. Singh, P. Chanak, and S. K. Singh, "Seizsclas: An efficient and secure internet-of-things-based eeg classifier," *IEEE Internet of Things Journal*, vol. 8, no. 8, pp. 6214–6221, 2020.

[8] R. Quintas, A. Raggi, A. M. Giovannetti, M. Pagani, C. Sabariego, A. Cieza, and M. Leonardi, "Psychosocial difficulties in people with epilepsy: a systematic review of literature from 2005 until 2010," *Epilepsy & Behavior*, vol. 25, no. 1, pp. 60–67, 2012.

[9] G. G. Celesia and R.-C. Chen, "Parameters of spikes in human epilepsy." *Diseases of the nervous system*, vol. 37, no. 5, pp. 277–281, 1976.

[10] A. K. Jaiswal and H. Banka, "Local pattern transformation based feature extraction techniques for classification of epileptic eeg signals," *Biomedical Signal Processing and Control*, vol. 34, pp. 81–92, 2017.

[11] O. Fasil and R. Rajesh, "Time-domain exponential energy for epileptic eeg signal classification," *Neuroscience letters*, vol. 694, pp. 1–8, 2019.

[12] G. S. Ohannesian and E. J. Harfash, "Epileptic seizures detection from eeg recordings based on a hybrid system of gaussian mixture model and random forest classifier," *Informatica*, vol. 46, no. 6, pp. 105–116, 2022.

[13] S. Lahmiri and A. Shmuel, "Accurate classification of seizure and seizure-free intervals of intracranial eeg signals from epileptic patients," *IEEE Transactions on Instrumentation and Measurement*, vol. 68, no. 3, pp. 791–796, 2018.

[14] Y. Jeon, Y. G. Chung, T. Joo, H. Kim, H. Hwang, and K. J. Kim, "Deep learning-based detection of epileptiform discharges for self-limited epilepsy with centrotemporal spikes," *IEEE Transactions on Neural Systems and Rehabilitation Engineering*, vol. 30, pp. 2939–2949, 2022.

[15] Y. Du and J. Liu, "Ienet: a robust convolutional neural network for eeg based brain-computer interfaces," *Journal of Neural Engineering*, vol. 19, no. 3, p. 36031, 2022.

[16] P. Dhar, V. K. Garg, and M. A. Rahman, "Enhanced feature extraction-based cnn approach for epileptic seizure detection from eeg signals," *Journal of Healthcare Engineering*, vol. 2022, p. 3491828, 2022.

[17] E. Tuncer and E. D. Bolat, "Classification of epileptic seizures from electroencephalogram (eeg) data using bidirectional short-term memory (bi-lstm) network architecture," *Biomedical Signal Processing and Control*, vol. 73, p. 103462, 2022.

[18] A. Çalışkan, "A new ensemble approach for congestive heart failure and arrhythmia classification using shifted one-dimensional local binary patterns with long short-term memory," *The Computer Journal*, vol. 65, no. 9, pp. 2535–2546, 2022.

[19] K. S. Shekokar and S. Dour, "Automatic epileptic seizure detection using lstm networks," *World Journal of Engineering*, vol. 19, no. 2, pp. 224–229, 2021.

[20] M. Varlı and H. Yılmaz, "Multiple classification of eeg signals and epileptic seizure diagnosis with combined deep learning," *Journal of Computational Science*, vol. 67, p. 101943, 2023.

[21] X. Qiu, F. Yan, and H. Liu, "A difference attention resnet-lstm network for epileptic seizure detection using eeg signal," *Biomedical Signal Processing and Control*, vol. 83, p. 104652, 2023.

[22] A. Lebal, A. Moussaoui, and A. Rezgui, "Epilepsy-net: attention-based 1d-inception network model for epilepsy detection using one-channel and multi-channel eeg signals," *Multimedia Tools and Applications*, vol. 82, no. 11, pp. 17 391–17 413, 2023.

[23] I. Ahmad, X. Wang, M. Zhu, C. Wang, Y. Pi, J. A. Khan, S. Khan, O. W. Samuel, S. Chen, and G. Li, "Eeg-based epileptic seizure detection via machine/deep learning approaches: A systematic review," *Computational Intelligence and Neuroscience*, vol. 2022, p. 6486570, 2022.

[24] P. Nejedly, V. Kremen, K. Lepkova, F. Mivalt, V. Sladky, T. Pridalova, F. Plesinger, P. Jurak, M. Pail, M. Brazdil *et al.*, "Utilization of temporal autoencoder for semi-supervised intracranial eeg clustering and classification," *Scientific reports*, vol. 13, no. 1, p. 744, 2023.

[25] A. Shoeibi, N. Ghassemi, M. Khodatars, P. Moridian, R. Alizadehsani, A. Zare, A. Khosravi, A. Subasi, U. R. Acharya, and J. M. Gorriz, "Detection of epileptic seizures on eeg signals using anfis classifier, autoencoders and fuzzy entropies," *Biomedical Signal Processing and Control*, vol. 73, p. 103417, 2022.

[26] Y. Qiu, W. Zhou, N. Yu, and P. Du, "Denoising sparse autoencoder-based ictal eeg classification," *IEEE Transactions on Neural Systems and Rehabilitation Engineering*, vol. 26, no. 9, pp. 1717–1726, 2018.

[27] K. A. Schindler and A. Rahimi, "A primer on hyperdimensional computing for ieeg seizure detection," *Frontiers in neurology*, vol. 12, p. 701791, 2021.

[28] P. Kanerva, "Hyperdimensional computing: An introduction to computing in distributed representation with high-dimensional random vectors," *Cognitive computation*, vol. 1, pp. 139–159, 2009.

[29] L. Ge and K. K. Parhi, "Classification using hyperdimensional computing: A review," *IEEE Circuits and Systems Magazine*, vol. 20, no. 2, pp. 30–47, 2020.

[30] A. Rahimi, S. Datta, D. Kleyko, E. P. Frady, B. Olshausen, P. Kanerva, and J. M. Rabaey, "High-dimensional computing as a nanoscalable paradigm," *IEEE Transactions on Circuits and Systems I: Regular Papers*, vol. 64, no. 9, pp. 2508–2521, 2017.

[31] U. Pale, T. Teijeiro, and D. Atienza, "Multi-centroid hyperdimensional computing approach for epileptic seizure detection," *Frontiers in Neurology*, vol. 13, p. 816294, 2022.

[32] U. Pale, T. Teijeiro, S. Rheims, P. Ryvlin, and D. Atienza, "Combining general and personal models for epilepsy detection with hyperdimensional computing," *Artificial Intelligence in Medicine*, p. 102754, 2024.

[33] L. Ge and K. K. Parhi, "Applicability of hyperdimensional computing to seizure detection," *IEEE Open Journal of Circuits and Systems*, vol. 3, pp. 59–71, 2022.

[34] U. Pale, T. Teijeiro, and D. Atienza, "Exg signal feature selection using hyperdimensional computing encoding," in *2022 IEEE International Conference on Bioinformatics and Biomedicine (BIBM)*. IEEE, 2022, pp. 1688–1693.

[35] F. Asgarinejad, A. Thomas, and T. Rosing, "Detection of epileptic seizures from surface eeg using hyperdimensional computing," in *2020 42nd Annual International Conference of the IEEE Engineering in Medicine & Biology Society (EMBC)*. IEEE, 2020, pp. 536–540.

[36] U. Pale, T. Teijeiro, and D. Atienza, "Systematic assessment of hyperdimensional computing for epileptic seizure detection," in *2021 43rd Annual International Conference of the IEEE Engineering in Medicine & Biology Society (EMBC)*. IEEE, 2021, pp. 6361–6367.

[37] G. Zhang, X. Huang, S. Z. Li, Y. Wang, and X. Wu, "Boosting local binary pattern (lbp)-based face recognition." in *Sinobiometrics*. Springer, 2004, pp. 179–186.

[38] C. S. Daw, C. E. A. Finney, and E. R. Tracy, "A review of symbolic analysis of experimental data," *Review of Scientific instruments*, vol. 74, no. 2, pp. 915–930, 2003.

[39] A. Burrello, K. Schindler, L. Benini, and A. Rahimi, "Hyperdimensional computing with local binary patterns: One-shot learning of seizure onset and identification of ictogenic brain regions using short-time ieeg

recordings," *IEEE Transactions on Biomedical Engineering*, vol. 67, no. 2, pp. 601–613, 2019.
[40] A. Burrello, L. Cavigelli, K. Schindler, L. Benini, and A. Rahimi, "Laelaps: An energy-efficient seizure detection algorithm from long-term human ieeg recordings without false alarms," in *2019 Design, Automation & Test in Europe Conference & Exhibition (DATE)*. IEEE, 2019, pp. 752–757.
[41] A. H. Shoeb and J. V. Guttag, "Application of machine learning to epileptic seizure detection," in *Proceedings of the 27th international conference on machine learning (ICML)*, 2010, pp. 975–982.
[42] S. Wolfram, "Random sequence generation by cellular automata," *Advances in applied mathematics*, vol. 7, no. 2, pp. 123–169, 1986.
[43] M. Ancona, E. Ceolini, C. Öztireli, and M. Gross, "Towards better understanding of gradient-based attribution methods for deep neural networks," *arXiv preprint arXiv:1711.06104*, 2017.
[44] L. Van der Maaten and G. Hinton, "Visualizing data using t-sne." *Journal of machine learning research*, vol. 9, no. 11, pp. 2579–2605, 2008.
[45] W. Nasreddine, "Epileptic eeg dataset," 2021. [Online]. Available: https://doi.org/10.17632/5pc2j46cbc.1.
[46] C. Zhang, Y.-K. Kim, and A. Eskandarian, "Eeg-inception: an accurate and robust end-to-end neural network for eeg-based motor imagery classification," *Journal of Neural Engineering*, vol. 18, no. 4, p. 46014, 2021.
[47] C.-P. Shen, S.-T. Liu, W.-Z. Zhou, F.-S. Lin, A. Y.-Y. Lam, H.-Y. Sung, W. Chen, J.-W. Lin, M.-J. Chiu, M.-K. Pan *et al.*, "A physiology-based seizure detection system for multichannel eeg," *PloS one*, vol. 8, no. 6, p. e65862, 2013.
[48] F. E. Abd El-Samie, T. N. Alotaiby, M. I. Khalid, S. A. Alshebeili, and S. A. Aldosari, "A review of eeg and meg epileptic spike detection algorithms," *IEEE Access*, vol. 6, pp. 60 673–60 688, 2018.
[49] R. Esteller, J. Echauz, T. Tcheng, B. Litt, and B. Pless, "Line length: an efficient feature for seizure onset detection," in *2001 Conference Proceedings of the 23rd Annual International Conference of the IEEE Engineering in Medicine and Biology Society*, vol. 2. IEEE, 2001, pp. 1707–1710.
[50] A. Burrello, S. Benatti, K. Schindler, L. Benini, and A. Rahimi, "An ensemble of hyperdimensional classifiers: hardware-friendly short-latency seizure detection with automatic ieeg electrode selection," *IEEE journal of biomedical and health informatics*, vol. 25, no. 4, pp. 935–946, 2020.
[51] M. Schmuck, L. Benini, and A. Rahimi, "Hardware optimizations of dense binary hyperdimensional computing: Rematerialization of hypervectors, binarized bundling, and combinational associative memory," *ACM Journal on Emerging Technologies in Computing Systems (JETC)*, vol. 15, no. 4, pp. 1–25, 2019.
[52] S. Jenssen, E. J. Gracely, and M. R. Sperling, "How long do most seizures last? a systematic comparison of seizures recorded in the epilepsy monitoring unit," *Epilepsia*, vol. 47, no. 9, pp. 1499–1503, 2006.
[53] J. Liu, M. Ma, Z. Zhu, Y. Wang, and H. Yang, "Hdc-im: Hyperdimensional computing in-memory architecture based on rram," in *2019 26th IEEE International Conference on Electronics, Circuits and Systems (ICECS)*. IEEE, 2019, pp. 450–453.
[54] W. Wu, H. Wu, B. Gao, P. Yao, X. Zhang, X. Peng, S. Yu, and H. Qian, "A methodology to improve linearity of analog rram for neuromorphic computing," in *2018 IEEE symposium on VLSI technology*. IEEE, 2018, pp. 103–104.
[55] X. Peng, S. Huang, H. Jiang, A. Lu, and S. Yu, "Dnn+ neurosim v2. 0: An end-to-end benchmarking framework for compute-in-memory accelerators for on-chip training," *IEEE Transactions on Computer-Aided Design of Integrated Circuits and Systems*, vol. 40, no. 11, pp. 2306–2319, 2020.
[56] A. Lu, X. Peng, W. Li, H. Jiang, and S. Yu, "Neurosim simulator for compute-in-memory hardware accelerator: Validation and benchmark," *Frontiers in artificial intelligence*, vol. 4, p. 659060, 2021.
[57] C. Li, C. Lammie, X. Dong, A. Amirsoleimani, M. R. Azghadi, and R. Genov, "Seizure detection and prediction by parallel memristive convolutional neural networks," *IEEE Transactions on Biomedical Circuits and Systems*, vol. 16, no. 4, pp. 609–625, 2022.
[58] C. Lammie, W. Xiang, and M. R. Azghadi, "Towards memristive deep learning systems for real-time mobile epileptic seizure prediction," in *2021 IEEE International Symposium on Circuits and Systems (ISCAS)*. IEEE, 2021, pp. 1–5.
[59] T. Zhan, S. Guraya, and H. Kassiri, "A resource-optimized vlsi architecture for patient-specific seizure detection using frontal-lobe eeg," in *2019 IEEE international symposium on circuits and systems (ISCAS)*. IEEE, 2019, pp. 1–5.
[60] Y. Wen, Y. Zhang, L. Wen, H. Cao, G. Ai, M. Gu, P. Wang, and H. Chen, "A 65nm/0.448 mw eeg processor with parallel architecture svm and lifting wavelet transform for high-performance and low-power epilepsy detection," *Computers in Biology and Medicine*, vol. 144, p. 105366, 2022.
[61] G. Ai, Y. Zhang, Y. Wen, M. Gu, H. Zhang, and P. Wang, "Convolutional neural network-based lightweight hardware ip core design for eeg epilepsy prediction," *Microelectronics Journal*, vol. 137, p. 105810, 2023.
[62] Y. Su, W. Shi, L. Hu, and S. Zhuang, "Implementation of svm-based low power eeg signal classification chip," *IEEE Transactions on Circuits and Systems II: Express Briefs*, vol. 69, no. 10, pp. 4048–4052, 2022.
[63] J. Yoo, L. Yan, D. El-Damak, M. A. B. Altaf, A. H. Shoeb, and A. P. Chandrakasan, "An 8-channel scalable eeg acquisition soc with patient-specific seizure classification and recording processor," *IEEE journal of solid-state circuits*, vol. 48, no. 1, pp. 214–228, 2012.

Yipeng Du received the B.E. degree in Communication Engineering from University of Science and Technology Beijing and M.E. degree in Signal and Information Processing from Peking University. He is currently pursuing the Ph.D. degree with the Department of Electrical and Electronic Engineering, The University of Hong Kong, Hong Kong, SAR. His current research interests include EEG-based brain-computer interface, machine learning, and signal processing.

Yuan Ren received the M.S. degree in electrical and computer engineering from the University of Macau (UM), Macao, China in 2016. He is currently pursuing the Ph.D. degree in electrical and electronic engineering from the University of Hong Kong (HKU). His research focuses on algorithm-hardware co-design for AI accelerator and memristor-based compute-in-memory integrated circuits. He joined the State Key Laboratory of Analog and Mixed-Signal VLSI, University of Macau, since 2017, working on the design of low-power analog integrated circuit. He then joined the SoC Key Laboratory, Peking University Shenzhen Institute and PKU-HKUST Shenzhen-Hong Kong Institution, Guangdong, China, in 2018. His research interests include data converters and power management circuits. Mr. Ren received the Excellent Postgraduate Student of the University of Macau Award in 2017. He served as a reviewer for multiple IEEE journals.

Ngai Wong (Senior Member, IEEE) received the B.Eng. and Ph.D. degrees in electrical and electronic engineering from The University of Hong Kong (HKU), Hong Kong. He was a Visiting Scholar with Purdue University, West Lafayette, IN, USA, in 2003. He is currently an Associate Professor with the Department of Electrical and Electronic Engineering, HKU. He was the Associate Editor of IEEE Transactions on Computer-Aided Design of Integrated Circuits and Systems from Jan 2014- Jun 2022, and has served as the track chair and member in the technical program committees (TPCs) of premier EDA conferences every year including DAC, ICCAD and ASP-DAC. He co-founded the IEEE Council on EDA (CEDA), Hong Kong Chapter in 2016, and was the Chair in 2018/19. His research interests include compact neural network design, compute-in-memory (CIM) AI chips, electronic design automation (EDA) and tensor algebra.

Edith C. H. Ngai (Senior Member, IEEE) received the Ph.D. degree from the Chinese University of Hong Kong, Hong Kong, China, in 2007. She is currently an Associate Professor with the Department of Electrical and Electronic Engineering, The University of Hong Kong (HKU), Hong Kong. Before joining HKU in 2020, she was an Associate Professor with the Department of Information Technology, Uppsala University, Uppsala, Sweden. Her research interests include Internet of Things, machine learning, data analytics, and smart cities. Dr. Ngai received a Meta Policy Research Award in Asia–Pacific in 2022. She was elected as one of the IEEE N2Women Stars in Computer Networking and Communications in 2022. She is an IEEE ComSoc Distinguished Lecturer from 2023 to 2024.